FULL PAPER

A quantitative comparison between a navigated Cartesian and a self-navigated radial protocol from clinical studies for free-breathing 3D whole-heart bSSFP coronary MRA

John Heerfordt[1,2] 🆔 | Matthias Stuber[1,3] 🆔 | Aurélien Maillot[1,2] | Veronica Bianchi[1] | Davide Piccini[1,2] 🆔

[1]Department of Diagnostic and Interventional Radiology, Lausanne University Hospital and University of Lausanne, Lausanne, Switzerland

[2]Advanced Clinical Imaging Technology, Siemens Healthcare AG, Lausanne, Switzerland

[3]Center for Biomedical Imaging (CIBM), Lausanne, Switzerland

Correspondence
Davide Piccini, Center for Biomedical Imaging, Centre Hospitalier Universitaire Vaudois, Rue du Bugnon 46, BH 7.82, 1011 Lausanne, Switzerland.
Email: piccinidavide@gmail.com; Twitter: @CVMR_Lausanne

Funding information
Schweizerischer Nationalfonds zur Förderung der Wissenschaftlichen Forschung, Grant/Award Number: 320030_143923

Purpose: Navigator-gated 3D bSSFP whole-heart coronary MRA has been evaluated in several large studies including a multi-center trial. Patient studies have also been performed with more recent self-navigated techniques. In this study, these two approaches are compared side-by-side using a Cartesian navigator-gated and corrected (CNG) and a 3D radial self-navigated (RSN) protocol from published patient studies.

Methods: Sixteen healthy subjects were examined with both sequences on a 1.5T scanner. Assessment of the visibility of coronary ostia and quantitative comparisons of acquisition times, blood pool homogeneity, and visible length and sharpness of the right coronary artery (RCA) and the combined left main (LM)+left anterior descending (LAD) coronary arteries were performed. Paired sample t-tests with $P < .05$ considered statistically significant were used for all comparisons.

Results: The acquisition time was $5:40 \pm 0:28$ min (mean $\pm$ SD) for RSN, being significantly shorter than the $16:59 \pm 5:05$ min of CNG ($P < .001$). RSN images showed higher blood pool homogeneity ($P < .001$). All coronary ostia were visible with both techniques. CNG provided significantly higher vessel sharpness in the RCA (CNG: $50.0 \pm 8.6\%$, RSN: $34.2 \pm 6.9\%$, $P < .001$) and the LM+LAD (CNG: $48.7 \pm 6.7\%$, RSN: $32.3 \pm 7.1\%$, $P < .001$). The visible vessel length was significantly longer in the LM+LAD using CNG (CNG: 9.8 ± 2.7 cm, RSN: 8.5 ± 2.6 cm, $P < .05$) but not in the RCA (CNG: 9.7 ± 2.3 cm, RSN: 9.3 ± 2.9 cm, $P = .29$).

Conclusion: CNG provided superior vessel sharpness and might hence be the better option for examining coronary lumina. However, its blood pool inhomogeneity and prolonged and unpredictable acquisition times compared to RSN may make clinical adoption more challenging.

KEYWORDS
bSSFP, coronary MRA, navigator-gating, self-navigation, whole-heart

1 | INTRODUCTION

Coronary magnetic resonance angiography (CMRA) is an appealing alternative to X-ray coronary angiography because it allows for non-invasive imaging without ionizing radiation. One thoroughly evaluated CMRA technique is respiratory navigator-gated ECG-triggered 3D whole-heart balanced steady state free precession (bSSFP) imaging at 1.5T, which has been used in patients both in a multicenter trial[1] and in large single-center studies.[2,3] Typically, such protocols include T_2-preparation[4] and fat-saturation[5,6] pre-pulses for contrast optimization and parallel imaging[7,8] to shorten the acquisition time. Respiratory gating using diaphragmatic navigator echoes[9] allows for only accepting readouts acquired during a specific respiratory phase, typically end-expiration. For prospective motion correction within the acceptance window, slice tracking has been developed.[10] Although navigator-gating is effective for mitigating respiratory motion artifacts, it has intrinsic drawbacks: namely the need to accurately plan the navigator position and its acceptance window, the high rate of discarded data, related time inefficiency, highly unpredictable scanning times, and the risk of aborted or incomplete scans because of respiratory drift. In the aforementioned multi-center study,[1] the average navigator acceptance efficiency was <40% despite the use of tight-fitting belts restricting respiratory motion,[11] and 8% of the acquisitions were not completed because of irregular breathing or diaphragmatic drift. Although images of high quality can be obtained with navigator-gated CMRA at specialized institutions, it remains challenging to include such protocols into the clinical workflow because of their limited ease-of-use, uncertainty in scan time, and risk of failure.

To address the above drawbacks of the navigator-gating paradigm and to facilitate the transition of CMRA into conventional clinical imaging, respiratory self-navigation that uses data acquired directly from the organ of interest to perform motion detection or correction has been suggested. It was first introduced in whole-heart CMRA by Stehning et al[12] who proposed a 3D radial sampling pattern where the first readout in each heartbeat consistently is oriented in the superior–inferior (SI) direction. By computing 1D projection images from such readouts and comparing these to one another, motion correction can be performed in k-space, which enables 100% acceptance of the acquired data.[12] Moreover, it reduces the time lag between motion detection and the actual data acquisition when compared to conventional navigators. Over the past few years, a wide range of different respiratory self-navigated CMRA techniques have been developed. These range from use of the start-up excitations[13] in bSSFP acquisitions to perform image-based motion correction[14] to sorting imaging data into different motion states and either perform motion correction[15] or use compressed sensing[16] to reconstruct motion-resolved images.[17] Experience in patients already exists for self-navigated techniques. A sequence similar to Stehning et al[12] but with more sophisticated motion detection[18] and a different 3D radial trajectory[19] has been used in some of the largest patient studies with self-navigated respiratory motion-correction to date,[20-22] reaching a total of ~300 subjects. More recently, image-based self-navigation has also been clinically evaluated with promising results.[23,24]

Navigator-gated and respiratory self-navigated whole-heart CMRA have co-existed for many years; therefore, a systematic side-by-side comparison using optimized protocols from large published patient studies is warranted. Our aim is to perform a quantitative comparison of these 2 techniques by replicating protocols from published patient studies as closely as possible and systematically acquiring these protocols in healthy volunteers. In particular, for the navigator-gated approach, a protocol adopted from a patient study by Sakuma et al[25] was chosen. Their landmark publication proved that whole-heart CMRA can be performed in <30 min in patients, including scout scans and cine imaging for resting phase detection. The imaging sequence is similar to those used in some of the earlier mentioned large trials.[1,3] This specific protocol was chosen because of its similarity to Kato et al[1] but being easier to replicate because of e.g., conventional centric-ordered Cartesian sampling and no use of respiratory belts. For the self-navigated reference, we selected the previously mentioned prototype 3D radial protocol that has been used in some of the largest patient studies with self-navigated techniques.[20-22] Preliminary results from this work were in part presented in abstract form at the Joint EuroCMR/SCMR Conference 2018.[26]

2 | METHODS

The objective of this study was to perform a quantitative comparison between the well-established navigator-gated and corrected Cartesian CMRA technique as described in Sakuma et al[25] and a more recently reported self-navigated 3D radial sequence.[20,21] Figure 1 illustrates the different building blocks of the two sequences while their main parameters are summarized in Table 1. Both the navigator-gated and the self-navigated protocols use segmented and ECG-triggered bSSFP sequences acquired during free-breathing. For every heartbeat, the data readout module is preceded by T_2-preparation (50 ms TE) and fat-saturation pre-pulses. In particular, chemically selective fat-suppression[6] (i.e., lipid frequency selective excitation followed by spoiling of transverse magnetization) with a total duration of 17 ms is used. Ten dummy excitations with linearly increasing startup angles (LISA)[13] precede the data acquisition during each heartbeat to reduce signal oscillations while approaching steady-state (duration: 10 repetition times). The published protocols were closely replicated, but some changes had to
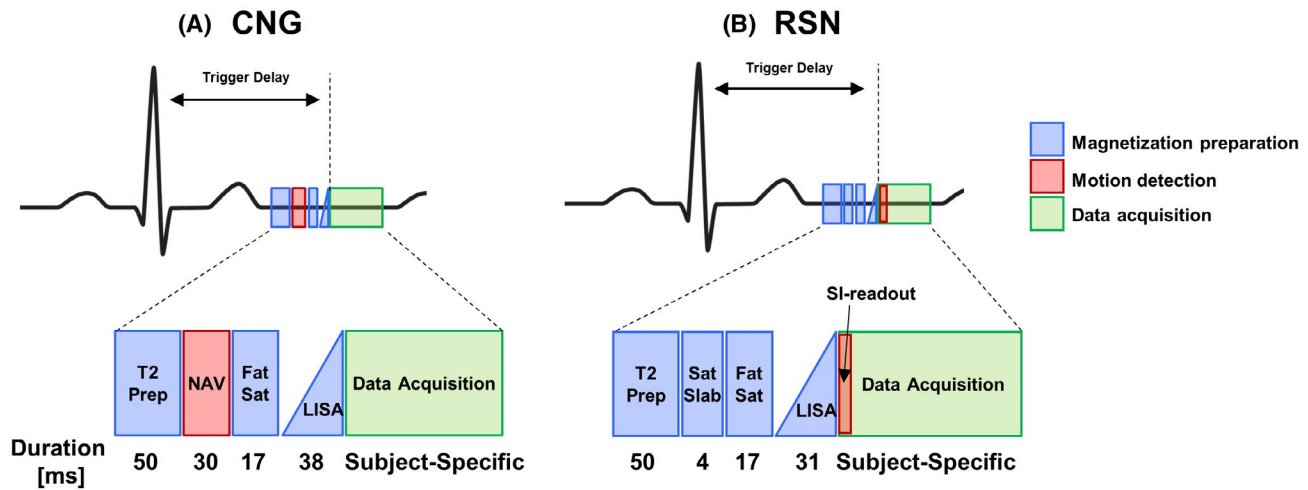
FIGURE 1 Overview of the Cartesian navigator-gated and corrected (CNG) and the radial self-navigated (RSN) sequence. The graphic outlines the different components of the 2 ECG-triggered sequences and their chronological order. Both CNG and RSN use T_2-preparation (T_2 Prep), and fat-saturation (Fat Sat) pre-pulses for contrast optimization and use ramp-up pulses (LISA) to reduce oscillations in the magnetization while approaching steady state. (A) In the CNG sequence a separate excitation and readout block is needed for the navigator-echo. (B) In the RSN sequence the motion detection is integrated into the data acquisition block by consistently orienting the first readout in each heartbeat in the superior-inferior (SI) direction. This allows for directly tracking the position of the heart instead of using indirect estimates based on the position of the diaphragm and also shortens the time lag from the moment when the heart's position is determined until the actual data acquisition. Moreover, RSN uses a saturation slab (Sat Slab) to suppress fat signal from the chest to facilitate self-navigation

be made because of different hardware, software, and/or vendor. For the navigator-gated sequence, GRAPPA[8] was used instead of SENSE,[7] which was used in the study from which the protocol was adopted. The self-navigated sequence did not use any parallel imaging for consistency with the associated patient studies. Moreover, some minor changes were made to facilitate the comparison such as matching the axial slice resolution and the RF excitation angle as well as homogenizing and increasing the readout bandwidth to shorten the echo and repetition times. Additionally, no contrast agent was administered.

2.1 | Cartesian navigator-gated and corrected protocol

To suppress respiratory motion artifacts, the Cartesian navigator-gated and corrected (CNG) acquisition (Figure 1A) uses a navigator[9] placed on the dome of right hemi-diaphragm. Slice tracking[10] is applied for motion correction within the manually selected 5 mm end-expiratory acceptance window, using the conventional tracking factor of 0.6^{27} to correlate diaphragmatic and cardiac displacements. The end-expiratory level is determined manually by considering which navigator-level at end-expiration is the most frequently occurring in a 10-s scout scan. The Cartesian sampling implements a centric ordering scheme for optimal fat suppression and contrast, and is accelerated by a factor 2 using GRAPPA[8] in the anterior–posterior (AP) phase encoding (PE) direction. The FOV is $280 \times 280 \times 120$ mm^3 (readout $\times$ AP PE $\times$ SI PE) with an

acquired anisotropic spatial resolution of $1.09 \times 1.09 \times 1.50$ mm^3, subsequently interpolated to $0.55 \times 0.55 \times 0.75$ mm^3 during the reconstruction. The same FOV, number of slices, and acquired resolution were used for all subjects for consistency with the published protocol.

2.2 | Radial self-navigated protocol

As part of the radial self-navigated (RSN) technique (Figure 1B), an automated segmentation of the blood pool along the Fourier transformed SI-readout acquired in every heartbeat allows for estimation of the cardiac blood pool position in 1D.[18] Thereafter, cross-correlation is used to compute the heart's position over time, which is used for inter-RR respiratory motion correction in k-space. To facilitate the blood pool segmentation, a spatial pre-saturation pulse[28] is used to suppress signal from the chest. The segmented 3D radial spiral phyllotaxis sampling scheme used in RSN was originally designed for acquiring k-space with an overall uniform readout distribution and to simultaneously minimize Eddy current effects.[19] An amount of data corresponding to ~20% of the radial Nyquist limit[29] is acquired (5-fold acceleration) and a density compensation function is used to balance the energy in k-space when re-gridding the radial data onto a Cartesian grid before inverse 3D Fourier transformation.[30] The influence of frequencies higher than the radial Nyquist limit is restricted by saturating the density compensation function.[30] The FOV is $210 \times 210 \times 210$ mm^3 (acquired as $420 \times 420 \times 420$ mm^3

TABLE 1 Sequence parameters

Parameter	Navigator-gated Cartesian protocol	Self-navigated radial protocol
Sampling scheme	3D Cartesian (centric ordering)	3D radial (spiral phyllotaxis)
Acceleration	GRAPPA, acceleration factor 2, 50% of Cartesian Nyquist limit acquired + 24 internal calibration lines	acceleration factor ~5, ~20% of radial Nyquist limit acquired
Nominal scan time (60 heartbeats/min, 100 ms acquisition window)	16:27 min (40% navigator efficiency)	6:14 min
FOV (mm^3)	$280 \times 280 \times 120$	$210 \times 210 \times 210$
Acquisition matrix	$256 \times 256 \times 80$ (no slice-oversampling)	$192 \times 192 \times 192$
Acquired resolution (mm^3)	$1.09 \times 1.09 \times 1.50$ (anisotropic)	$1.09 \times 1.09 \times 1.09$ (isotropic)
TE/TR (ms)	1.91/3.82	1.57/3.14
RF excitation angle and type	90° slab-selective sinc pulse, 1 ms duration, axial excitation slab	90° non-selective rectangular pulse, 0.3 ms duration
T_2-preparation (TE)	yes (50 ms)	yes (50 ms)
Fat suppression	conventional spectrally selective suppression (90° fat-selective excitation followed by spoiling)	conventional spectrally selective suppression (90° fat-selective excitation followed by spoiling), anterior saturation slab
Readout bandwidth	1028 Hz/pixel	1002 Hz/pixel
Reconstruction technique and coil combination	GRAPPA, sum-of-squares	non-uniform FFT with zero-filling, sum-of-squares

Abbreviation: FFT, Fast Fourier Transform.

because of the intrinsic 2-fold readout oversampling) with an acquired and reconstructed isotropic voxel size of 1.09 $\times$ 1.09 $\times$ 1.09 mm^3.

2.3 | Data acquisition

This study was approved by the IRB and all recruited volunteers provided written informed consent before participation. Data sets from $N = 16$ healthy subjects, i.e. without general health problems and without known history of cardiovascular disease, (age: 27.3 $\pm$ 4.5 y [mean $\pm$ sample SD throughout the paper], age range: 21–40 y) were acquired on a 1.5T clinical MRI (MAGNETOM Aera, Siemens Healthcare, Erlangen, Germany). An 18-channel chest coil and a 32-channel spine coil were used for signal reception. As a first step, scout images were obtained in the 3 orthogonal directions to localize the heart. Second, the quiescent mid-diastolic cardiac resting phase was identified on an axial bSSFP cine acquisition for determination of the trigger delay and length of the acquisition window. The cine acquisition was acquired during free-breathing using 3 signal averages. Main sequence parameters for the cine acquisition were as follows: Cartesian k-space sampling (linear ordering), 25 cardiac phases, GRAPPA (acceleration factor 2), FOV = 340 $\times$ 276 mm^2 (readout $\times$ PE), voxel size = 1.8 $\times$ 1.8 $\times$ 6 mm^3, radio frequency excitation

angle = 56°, TE/TR = 1.16/2.73 ms, receiver bandwidth = 930 Hz/pixel. The reconstructed temporal resolution of the cine acquisitions was on average 41.1 $\pm$ 6.9 ms (range = 28.4–51.5 ms). Finally, the CNG and RSN sequences were acquired in randomized order to avoid bias from e.g., fatigue effects. In all subjects, imaging targeted the mid-diastolic cardiac resting phase. The number of readouts acquired every heartbeat was adjusted independently for the 2 protocols according to the duration of the subjects' cardiac resting phases. Matching the length of the acquisition windows resulted in a different number of acquired readouts per heartbeat between the 2 sequences, because RSN uses a shorter non-selective excitation (Table 1). General information about the acquisition procedures such as the number of acquired readouts per heartbeat were recorded for retrospective analysis.

2.4 | Data analysis

To compare the efficiency of CNG and RSN, the acquisition times and CNG's navigator efficiency were recorded. For RSN, the range of respiratory motion that was motion-corrected was ascertained as well. In addition, the average length of the RR intervals in the accepted heartbeats was recorded independently for the 2 sequences and the corresponding heartrates computed.

General image characteristics in terms of image artifacts and contrast were examined visually. To subjectively evaluate the coronary delineation associated with the 2 methods, human visual image quality scoring was performed. All volumes were displayed in randomized order, one after another, in a dedicated graphical user interface, in which 2 blinded observers (senior scientists, M.S. and D.P., with 23 and 8 years of experience in coronary MRA, respectively) independently scored the image quality of the following coronary segments: left main (LM) as well as proximal, mid, and distal right coronary artery (RCA), left anterior descending (LAD) coronary artery, and left circumflex (LCX) coronary artery. Scores were assigned according to the scale in McConnell et al[31]: 0 = coronary artery not visible, 1 = coronary artery visible with markedly blurred borders or edges, 2 = coronary artery visible with moderately blurred borders or edges, 3 = coronary artery visible with mildly blurred borders or edges, 4 = coronary artery visible with sharply defined borders or edges. To assess whether the observers considered the ostia of the RCA and the LM to be visible, the number of non-zero scores for the corresponding segments were counted. For all segments, the scores for CNG and RSN were compared over all subjects using the scores from both observers. Both the median score/segment and the corresponding first and third quartile ranges and the average score/segment and the associated SD were computed. To assess the agreement between the 2 observers, a global Cohen's kappa score with linear weighting was computed over all the rated segments, subjects, and methods.

To quantify the inhomogeneity of the blood pool signal, the relative standard deviation (RSD) of the signal intensity was computed in a circular region of interest (ROI) of 2.2 cm in diameter placed in the ascending aorta at the level of the RCA ostium. The RSD in percent is simply defined as the standard deviation of the voxel intensities in the ROI (σ_{ROI}) divided by their mean value (μ_{ROI}): RSD = 100 × σ_{ROI}/μ_{ROI} [%]. Additionally, the contrast between blood and myocardium was measured by comparing the signal intensities in the above-mentioned blood ROIs to those from ROIs at the anterior part of the myocardium of the left-ventricle at a mid-myocardial level. The blood–myocardium contrast ratio was computed as ($\mu_{ROI, blood} - \mu_{ROI, myocardium})/\mu_{ROI, myocardium}$. To quantify the vessel conspicuity, the visible vessel length and sharpness of the RCA and the combined LM+LAD coronary arteries were analyzed using dedicated software (SoapBubble).[32] In the software, the coronary lumen's centerline was marked in axial reformats along the full visible vessel course. Subsequently, the sharpness of both the proximal 4 cm and the full visible course of the vessels were measured in the multiplanar reformats generated by the software, assuring matching anatomical zoom

level in the reformatted images from the 2 techniques. In brief, SoapBubble computes the vessel sharpness from a first-order derivative image of the multiplanar reformat. A sharpness value of 100% corresponds to maximum signal intensity change at the vessel border whereas a lower value indicates inferior border sharpness.

2.5 | Statistical analysis

Two-sided paired t-tests with $P < .05$ considered statistically significant were used for comparison of heartrates during the acquisitions, length of the mid-diastolic acquisition windows and acquisition times. For non-significant P-values close to 0.2 the corresponding 95% confidence intervals were computed. For every coronary segment that was graded for quality by the 2 observers, two-sided Wilcoxon signed-rank tests with $P < .05$ considered statistically significant were used for comparing the scores of CNG and RSN. For each segment, the scores for all subjects and from both observers were considered. Two-sided paired t-tests with $P < .05$ considered statistically significant were also used for the comparisons of signal homogeneity, blood-myocardium contrast, visible vessel length, and vessel sharpness.

3 | RESULTS

3.1 | Data acquisition

Image acquisition was successfully completed in all volunteers with both imaging sequences. The scanning time using RSN was significantly shorter than using CNG with average acquisition times of 5:40 ± 0:28 min (range = 4:44–6:19) and 16:59 ± 5:05 min (range = 10:47–30:36), respectively ($P < .001$) (Figure 2A). The average navigator efficiency of CNG was 43 ± 10% (range = 25–63) and the scan efficiency of RSN 100%. In 1 CNG acquisition, considerable diaphragmatic drift occurred, and the volunteer was requested to alter the breathing pattern to allow the acquisition to finish. In this particular case, the scan duration amounted to 30:36 min (outlier in Figure 2A). The range of corrected SI-oriented motion in the RSN acquisitions was on average 4.6 ± 2.5 mm (range = 1.09–9.81). The average heartrate during the CNG acquisitions was 60 ± 11 beats/min (range = 49–86) and during the RSN acquisitions 59 ± 11 beats/min (range = 48–82) ($P = .27$, 95% confidence interval for difference [−0.7, 2.3]). The effective acquisition window was on average 120.3 ± 21.2 ms (range = 84.0–141.3) for CNG and 119.3 ± 20.4 ms (range =81.6–141.3) for RSN ($P = .38$). This corresponded to the acquisition of 31.5 ± 5.5 (range = 22–37) readouts per heartbeat for CNG and 38.0 ± 6.5 (range = 26–45) readouts using RSN.
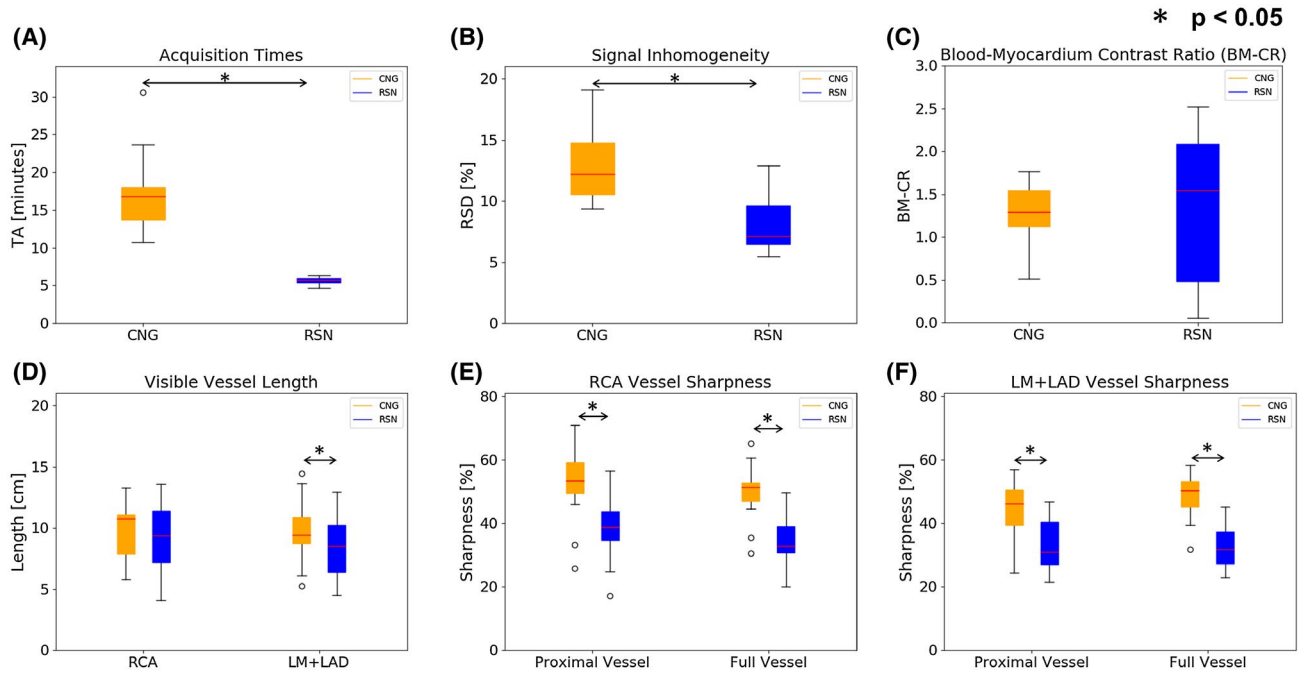
FIGURE 2 Quantitative results. (A) Acquisition times: the radial self-navigated sequence (RSN) finished on average approximately 3 times faster than its Cartesian navigator-gated and corrected (CNG) counterpart. (B) Blood pool inhomogeneity (RSD): RSN provided a more homogeneous blood pool in the ROI at the level of the RCA ostium. (C) Blood-myocardium contrast ratio (BM–CR): no significant differences were observed. (D) Visible vessel length: the visible vessel length of the LM+LAD was significantly longer using CNG whereas in the RCA non-significant differences were seen. (E) RCA vessel sharpness: CNG provided significantly sharper vessels. (F) LM+LAD vessel sharpness: CNG provided significantly sharper vessels

3.2 | Image characteristics

Visually, the 2 sequences produced images with different characteristics. Although the overall image contrast corresponded with the typical T_2/T_1 weighting consistent with bSSFP, differences were observed in terms of noise level, artifacts, fat-saturation, and image sharpness. Representative images from 2 volunteers are depicted in Figure 3. In the CNG images, the coronary arteries were in general clearly visible with good contrast relative to the myocardium and epicardial fat. However, the blood pool oftentimes appeared rather inhomogeneous and fold-over artifacts were frequently seen at the boundaries of the imaging volume in SI-direction, typically originating from the chest wall. Nevertheless, visual interface definition was often higher in CNG images relative to their RSN counterparts. In the latter, also the fat-suppression was suboptimal in some cases as demonstrated in subject A in Figure 4. In general, the RSN images appeared less noisy with a more homogeneous signal in the blood pool (Figures 3 and 5), and the presence of the typical radial streaking artifacts was low in the region of the heart (subject A in Figure 4). Also quantitatively, RSN images had a significantly more homogeneous signal in the blood ROI at the RCA ostium with an RSD of $8 \pm 2\%$ to be compared with $13 \pm 3\%$ of CNG (Figure 2B) ($P < .001$). In addition, RSN had better whole-heart coverage in the SI-direction because its FOV covered 21 cm (42 cm if the 2-fold readout

oversampling is used to reconstruct the full acquired FOV) to be compared to the 12 cm of CNG (subject B in Figure 4). No significant differences in blood-myocardium contrast ratio were seen between the 2 sequences ($P = .89$, Figure 2C).

3.3 | Assessment of the coronary arteries

The coronary ostia were visible in all subjects with both techniques. The results of the image quality scoring are summarized in Table 2. In brief, CNG obtained significantly higher scores for the mid RCA, mid and distal LAD, and distal LCX whereas RSN obtained significantly higher scores for the LM. The 2 observers showed a moderate global agreement with a Cohen's kappa of 0.58.

The visible vessel length was significantly longer for the combined LM+LAD using CNG (CNG: 9.8 ± 2.7 cm, RSN: 8.5 ± 2.6 cm, $P < .05$) but not for the RCA (CNG: 9.7 ± 2.3 cm, RSN: 9.3 ± 2.9 cm, $P = .29$, 95% confidence interval for difference [−0.36, 1.12]) (Figure 2D). However, CNG provided significantly sharper vessels, both in the proximal (CNG: $52.6 \pm 11.0\%$, RSN: $38.9 \pm 9.8\%$, $P < .001$) and full (CNG: $50.0 \pm 8.6\%$, RSN: $34.2 \pm 6.9\%$, $P < .001$) RCA as well as in the proximal (CNG: $44.2 \pm 8.2\%$, RSN: $32.8 \pm 8.0\%$, $P < .001$) and full (CNG: $48.7 \pm 6.7\%$, RSN: $32.3 \pm 7.1\%$, $P < .001$)
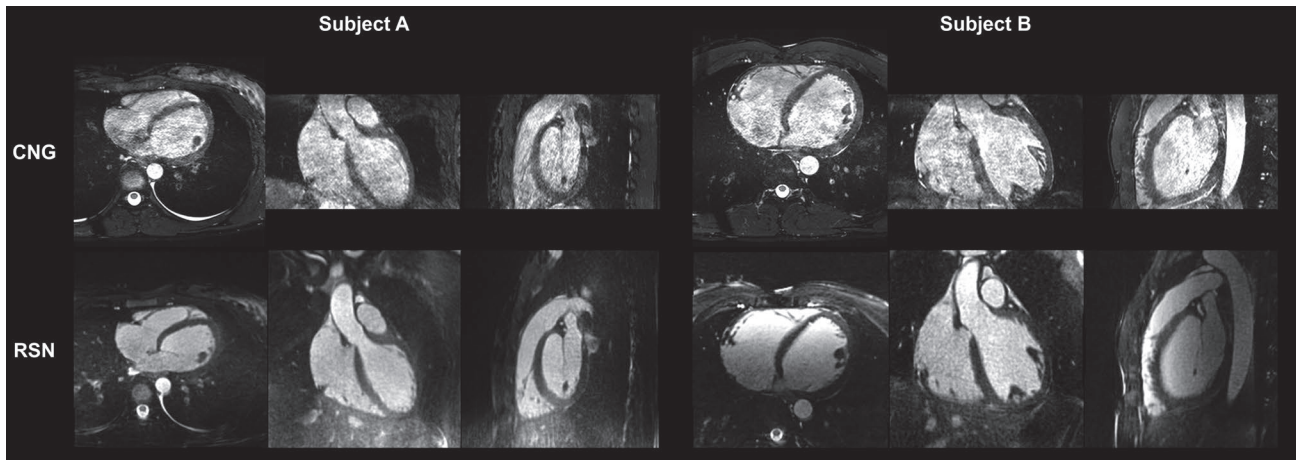
FIGURE 3 Representative images from the Cartesian navigator-gated and corrected (CNG) and the radial self-navigated (RSN) sequence. Representative example slices in the axial, coronal, and sagittal planes acquired with CNG (top) and RSN (bottom) from 2 subjects. The CNG images appear sharper but with a noisier blood pool. The RSN images are very smooth as a result of the intrinsic oversampling of low frequencies and undersampling of high spatial frequencies in k-space that characterize radial trajectories together with a density compensation function that assigns low weights to frequencies exceeding the radial Nyquist limit. Additionally, the rotating readout direction makes motion artifacts distribute in all spatial directions which also might contribute to the smoothness
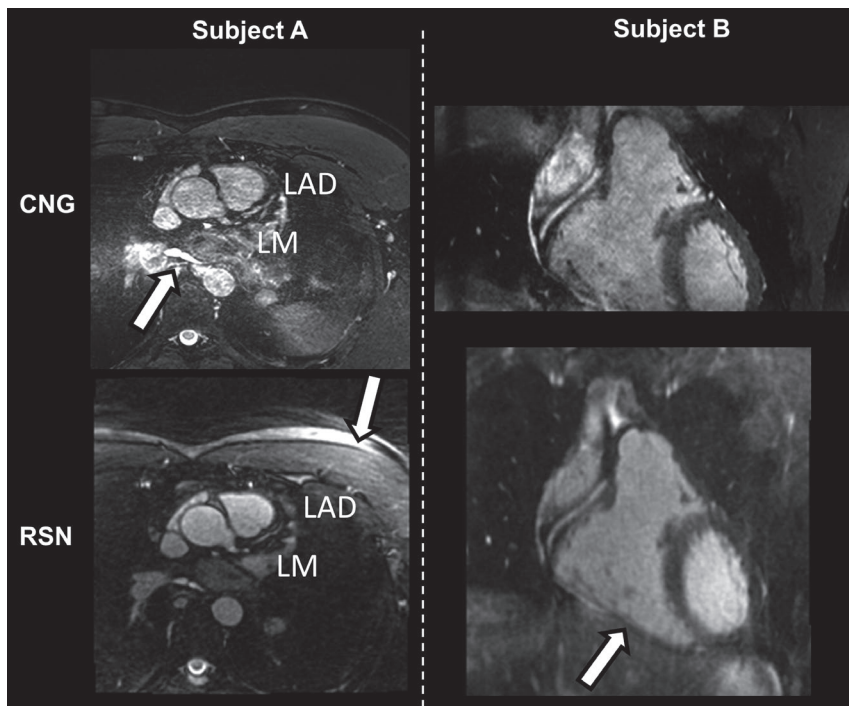

FIGURE 4 Typical image artifacts and characteristics. Subject A: at the level of the ostium of the LM fold-over can be seen in the Cartesian navigator-gated and corrected (CNG) image (lower left arrow) which decreases the perceived image quality even though the coronary origin still is visible. In the radial self-navigated (RSN) image, the inferior fat-saturation of radial acquisitions is demonstrated (upper right arrow) and moreover some typical streaking is seen. Subject B: in this large heart, the 12-cm coverage in SI-direction of CNG is too small, although it was consistent with the published protocol. A lower positioning of the axial slab would enable capturing the apex but at the expense of introducing fold-over at the coronary origins (slice-oversampling was not used). In the RSN image the whole heart is covered. The blurry heart-liver interface (arrow) points toward sub-optimal respiratory motion-correction in this particular case

LM+LAD (Figures 2E and F). Examples of multiplanar reformats of the RCA and the LM+LAD from 2 volunteers are depicted in Figure 5 where the visual impression corroborates the quantitative results (i.e., slightly better LM+LAD visible vessel length and much better vessel conspicuity using CNG).
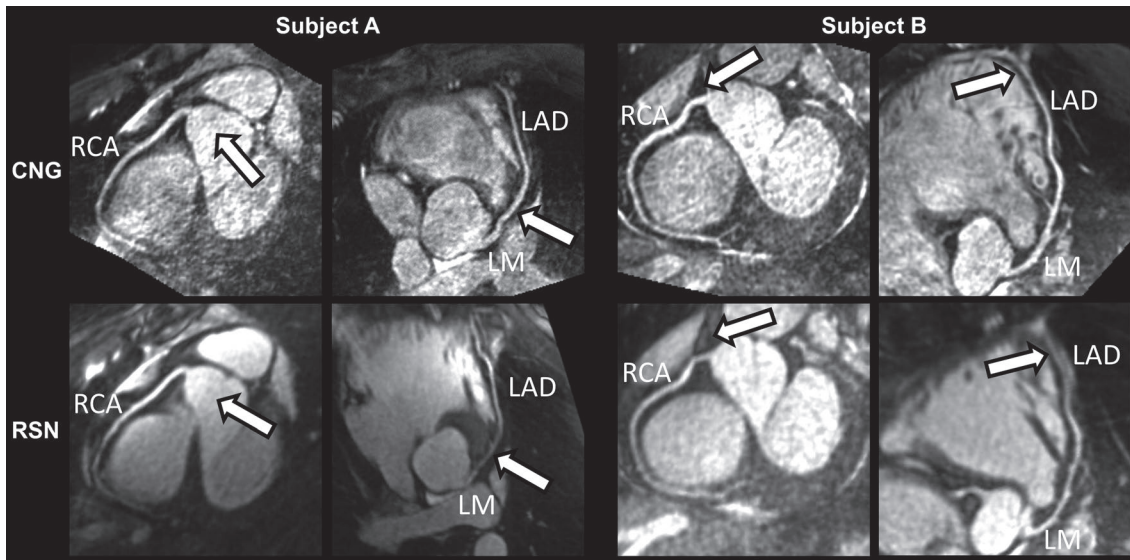
FIGURE 5 Multiplanar reformats of the RCA and LM+LAD from 2 different subjects. Overall, the quantitative superior vessel sharpness using the Cartesian navigator-gated and corrected (CNG) protocol as opposed to its radial self-navigated (RSN) counterpart appears to be reflected in the visually perceived vessel conspicuity. Subject A: quantitatively the blood pool inhomogeneity of RSN was measured to be lower, which agrees with the visual impression of the RCA reformats (arrows). In the LM + LAD, the vessel in the CNG image appears more conspicuous (arrows). Subject B: in the region of the proximal RCA a better fat saturation is observed with CNG as compared to RSN (region around arrows). In the LM+LAD the distal part of the vessel appears to be better depicted using CNG than RSN (arrows)

TABLE 2 Results of image quality scoring of coronary artery segments

Segment	Navigator-gated Cartesian protocol		Self-navigated radial protocol	
	Median [Q1, Q3]	Mean ± SD	Median [Q1, Q3]	Mean ± SD
RCA prox.	3 [2, 3][a]	2.5 ± 0.7[a]	2 [1, 3]	2.3 ± 1.2
RCA mid	2 [2, 3]*	2.3 ± 0.9[a]	2 [1, 3]	1.9 ± 1.0
RCA distal	1 [1, 2]	1.5 ± 1.2[a]	1 [0, 2]	1.1 ± 0.9
LM	2 [2, 3]	2.3 ± 0.6	3 [2, 3][a],*	2.7 ± 0.9[a]
LAD prox.	2 [2, 3]	2.25 ± 0.7	2 [2, 3]	2.3 ± 1.0[a]
LAD mid	2 [2, 3]*	2.3 ± 0.9[a]	2 [1, 2]	1.7 ± 0.9
LAD distal	2 [1, 2][a],*	1.6 ± 0.9[a]	1 [0, 1]	0.8 ± 0.8
LCX prox.	2 [2, 2.25]	2.0 ± 0.9[a]	2 [1, 3]	1.9 ± 1.0
LCX mid	1.5 [1, 2][a]	1.5 ± 1.0[a]	1 [0, 2]	1.2 ± 1.1
LCX distal	1 [0, 2][a],*	0.9 ± 1.0[a]	0 [0, 1]	0.5 ± 0.7

Abbreviations: LAD, Left Anterior Descending coronary artery; LCX, Left Circumflex coronary artery; LM, Left Main coronary artery; RCA, Right Coronary Artery.

The table contains the aggregated scores from both observers over all 16 subjects for every segment and method (i.e., 32 scores per segment per method). [Q1, Q3] = first and third quartiles.

[a]Higher median/mean.

*$P < .05$, Wilcoxon signed-rank test.

4 | DISCUSSION

This work aimed at the quantitative evaluation of strengths and weaknesses of CNG and RSN in a cohort of healthy adult subjects. The former provided superior depiction of the coronary arteries as measured both by subjective human image quality scoring and through more objective quantitative measures of vessel sharpness and length, but this came at the cost of severely prolonged and unpredictable acquisition times. The RSN protocol resulted in shorter and more predictable scan times and in images with a more homogeneous blood pool. Although a systematic evaluation of individual sequence characteristics was not the focus of this study that aimed at characterizing and comparing 2 well-established 3D whole-heart coronary MRA protocols, potential contributors to the above differences are discussed below.

The respiratory motion suppression strategies undoubtedly affect both the acquisition times and the conspicuity of the coronary arteries in the reconstructed images. The scan durations are intrinsically shorter using RSN, because all respiratory positions are accepted. This also results in highly predictable acquisition times as the main factors that may alter the *a priori* estimated scan duration are heart rate variability and missed ECG-triggers. For CNG, the total acquisition time is unknown until the data collection has finished as individual breathing patterns and potential diaphragmatic drift have a high impact on the navigator efficiency,[33] that in our study was similar to that in the previously mentioned multi-center study.[1] Regarding the vessel conspicuity, both techniques rely on 1D motion detection that has been proven to be sub-optimal in certain subjects.[14] Nevertheless, the range of SI-directed diaphragmatic motion that the slice tracking corrects for in CNG is only ±2.5 mm, which corresponds to cardiac displacements of approximately ±1.5 mm (assuming a 0.6 correlation), as opposed to the full respiratory range for the motion correction of RSN. Hence the smaller range of motion that has to be corrected for with CNG may contribute to a superior vessel sharpness. In addition, it has been shown for RSN that respiratory outlier positions degrade image quality[34] and consequently, the 100% data acceptance may have a negative influence on vessel conspicuity. On the other hand, RSN should be less sensitive than CNG to hysteresis in the diaphragm's level between inspiration and expiration with respect to the heart's position,[35] as the motion information is derived directly from the heart itself and not indirectly from the diaphragm as is the case for CNG. In a study that compared navigator-gated and self-navigated 3D radial coronary MRA, a high correlation was found between the respiratory displacement measurements and a tendency toward higher coronary vessel sharpness was seen when using the self-navigated technique.[18] That result suggests that the sharpness difference obtained in our study was not solely caused by the respiratory motion suppression techniques. Nevertheless, the visible vessel length is likely to be affected by the different motion suppression techniques. Using the CNG protocol, the prolonged acquisition time increases the risk for bulk motion. In addition, the correction factor of 0.6 originates from the findings in Wang et al[27] and is based on the displacement of the RCA ostium. Consequently, the potentially less accurate description of the respiratory displacement of more distal coronary segments might compromise the overall visible vessel course. For RSN, it has previously been concluded that technical improvements are needed to enhance the depiction of the distal coronary segments, as the motion correction relying on 1D motion detection in the SI-direction may not sufficiently account for the complexity of the respiratory displacement of the whole heart.[20] One possibility for overcoming this limitation might be non-rigid motion correction, which has been used in CMRA with promising results.[36-38] Last, it should be remembered that any kind of rigid motion correction, including CNG's slice tracking and RSN's phase modulation, turn static structures into moving structures that may generate artifacts and noise. In particular static adipose tissue, with high signal intensity in bSSFP images, may give rise to artifacts when it becomes subject to global motion correction. Such artifacts would appear more coherent in Cartesian images, but well saturated signal from adipose tissue, which here was achieved with the fat-saturated centric-ordered CNG sequence, should help to minimize that problem.

The second major factor that may impact the vessel conspicuity is the different k-space sampling schemes. An intrinsic property of 3D radial trajectories is that the sampling density is much higher near the k-space center than in the periphery. As a consequence, a density compensation function is used to balance the k-space energy content, and the choice of its parameters impacts the sharpness of the vessel borders and the signal homogeneity. As a matter of fact, the degree of sampling is very different between the 2 protocols. The CNG acquisition is only undersampled by a factor 2 whereas our RSN implementation is undersampled by approximately a factor of 5. It should be emphasized that 3 times more data could have been acquired with RSN if the acquisition times would have been matched to those of CNG. The 3D radial trajectory of RSN may also introduce blurriness, because its readout direction rotates. This makes motion artifacts spread across all spatial directions instead of appearing as distinct ghosting patterns and increases the sensitivity to trajectory and phase errors caused by Eddy currents and non-precise gradient delays. At the same time, off-resonance effects have a different impact depending on the sampling scheme. With Cartesian sampling they result in a linear spatial shift because all the acquired readouts are performed in the same spatial direction while for radial sampling the effect is different in every readout because the readout direction continuously changes. Additionally, the different sampling schemes affect the image contrast. The centric ordering in the CNG protocol allows for acquisition of low frequencies in k-space only in close proximity to the T_2-preparation and fat-saturation pre-pulses. With RSN on the other hand, each readout passes through the center of k-space, meaning that also those acquired more distant from the preparation pulses will sample low frequencies. Hence, data acquired with different time delay relative to the preparation pulses will be used for creating the final image. This is an intrinsic disadvantage associated with radial imaging, resulting in reduced contrast between blood and surrounding tissues and less saturated fat signal when compared to its centric-ordered Cartesian counterpart. Inadequate suppression of epicardial fat may result in lower coronary vessel sharpness. However, the difference in fat suppression between

CNG and RSN observed in this study may have been amplified by the long acquisition windows that the healthy subjects' diastolic resting phases allowed for. With a shorter acquisition window, as typically would be the case in patients, the time between the fat-saturation pre-pulse and the last readout in each heartbeat would be reduced.

In addition to the respiratory motion suppression and k-space sampling patterns, there are other differences between the 2 protocols such as the acquired voxel size and the type of excitation that may impact the image characteristics. The ~38% larger acquired voxel size of CNG provides an additional signal-to-noise advantage, on top of its Cartesian centric ordered sampling. Furthermore, the non-selective excitation pulse used in RSN may emphasize signal from structures outside the FOV, but may also reduce the inflow contrast by exciting blood magnetization outside of the imaged FOV. Concerning the homogeneity of the blood pool, the superiority of the radial acquisition might be attributed to its repetitive sampling of low frequencies in k-space, the low-pass filtering effect of the cut-off of the density compensation function, and the non-selective excitation that enables shorter echo times, therefore reducing the sensitivity to flow artifacts. In addition, Eddy currents associated with CNG's centric-ordering could be a contributing factor to its noisy blood pool. That no significant changes were observed in the blood-myocardium contrast ratio between CNG and RSN might be because of the fact that although the centric-ordered CNG makes better use of the T_2-preparation pre-pulse, it simultaneously results in less homogeneous signal which might reduce the measured contrast difference. In addition, the inter-subject variability in the dynamic range of the RSN images might have contributed to the large fluctuations seen in the used contrast measure. The slab-selective CNG provided a more similar dynamic range across subjects that might have contributed to its more consistent contrast values.

In our study, we found that both protocols have advantages and drawbacks and consequently the preference of one or the other depends on the aim of a particular examination and practical limitations such as available time. For examining congenital anomalies, especially malformations at the coronary origins,[39] both approaches might be adequate because the ostia could be seen in all subjects. Hence, RSN might be the method of choice because of its shorter and highly predictable acquisition time and cubic FOV. As a matter of fact, it has already showed promising results in congenital heart disease patients.[21,40] However, if the goal is to examine luminal narrowing, CNG may be the preferred alternative because of its superior coronary image quality scores and vessel sharpness. Still, that advantage has to be weighed against drawbacks such as the anisotropic voxel size that makes arbitrary reformatting more challenging (this can be important as studied in Botnar et al)[41]

and the long and unpredictable acquisition times. In the publications from which the protocols were adopted,[20,25] the per vessel sensitivity and specificity for detection of coronary artery stenosis were 82% and 91% for CNG and 65% and 85% with RSN. Although the seemingly better performance of CNG agrees with the visually more conspicuous and quantitatively sharper coronary arteries seen in this study, that comparison remains inadequate as different patient cohorts with different selection criteria were included in those publications. In the CNG study, the referred patients were suspected of having coronary artery disease, whereas the RSN study simply enrolled all patients referred to cardiac MR. Because bright blood whole-heart images can be used to examine anatomical structures other than the coronaries, several additional factors might be taken into consideration when deciding for a protocol to be used in a clinical setting. A homogeneous blood pool, as obtained with RSN, can be of particular interest in pediatric patients because it affects the possibility to examine vascular structures such as the pulmonary veins' connections with the left atrium.[42] Additionally, the larger coverage in the SI-direction of RSN simplifies planning and allows for examinations of the aortic arch. The 12 cm coverage of the CNG protocol is too small for such examinations and it is also problematic in subjects with a large heart because it might be difficult to capture both the coronary origins and their distal parts without changing readout and fold-over directions or extending the FOV. Increasing the FOV for CNG either mandates increased voxel size or prolonged acquisition time.

4.1 | Study limitations and future directions

This study has several limitations. First of all, the study was performed in healthy subjects only, and hence we can only speculate about the performance that one should expect in patients. The detection rate of stenosis using the 2 techniques compared to reference x-ray angiograms or coronary CT angiography would be an interesting future study (e.g., using similar metrics as Yang et al[43]). In our cohort of healthy subjects, such a comparison was not ethically justifiable and stenoses were not expected.

Another limitation is that we obtained vessel sharpness measures from 2 sequences with different acquired and reconstructed resolutions. We tried to minimize the influence thereof by zooming to the same anatomy for both CNG and RSN in the multiplanar reformatted image from which the sharpness is computed in SoapBubble.[32] Because the software uses reformats with a fixed number of pixels, this assures approximately the same resolution between the 2 sequences at the stage where the sharpness is computed.

Moreover, the compared protocols are not necessarily the most advanced among those published in the literature. However, as already stated in the introduction, they reflect techniques for which there exist a considerable amount of experience in patients. It was one of the major study design questions to choose which particular implementations of navigator-gating and respiratory self-navigation to compare. We decided to compare protocols that had been used in large patient studies while only matching some of the parameters such as the fat-sat and T_2-prep pre-pulses, the number of LISA dummy echoes, the acquired resolution in the axial plane, flip angle, readout bandwidth and coil-combination method. Alternatively, one could have matched the highest number of parameters possible both on the acquisition and the reconstruction side between the 2 techniques or used the very latest new technical developments. Indeed, several strategies exist that, if adopted, could have improved the performance of both CNG and RSN (e.g., belts constraining respiratory motion,[11] vasodilators,[44] and the administration of contrast medium[45]).

Specifically for CNG, drift-correction could have been used to improve the navigator efficiency to shorten the scan times, although it might compromise image quality because a wider range of anatomic positions would be accepted. Moreover, partial Fourier techniques would have allowed for reducing the amount of data that had to be acquired, at the expense of reduced signal-to-noise. If CNG would have used slice-oversampling, at least some of the fold-over artifacts that were seen in the peripheral slices of the axial slab might have been reduced, although at the cost of longer scan times. The presence of residual fold-over might be the reason that RSN obtained higher scores from the observers for the LM (the coronary artery with the most cranial position) and might also be one factor contributing to the overall noisiness of the CNG images. In addition, saturation slabs, could have been used also for CNG to better suppress signal from static tissues and reduce fold-over in the anterior–posterior phase encoding direction. Because CNG's centric ordering might induce high sensitivity to transient magnetization, it would also have been of interest to carefully optimize the number of LISA dummy echoes.

For RSN, the density compensation function is a very important parameter because it determines the balance between low and high frequencies. Here, we used the same one as in the patient studies with RSN, but it is possible that optimizing this function would lead to improved image quality. Moreover, reconstructing the acquired RSN data in a respiratory motion-resolved manner using compressed sensing,[16] has already proven to improve the vessel conspicuity.[17] Additionally, 3D radial SENSE has been described,[46] but in this study, parallel imaging was only used for accelerating CNG, which may be considered unfair

from a technical standpoint. Reconstructing both types of acquisitions with the same parallel imaging method, such as iterative SENSE[47] or SPIRiT,[48] may lead to an interesting comparison.

As an alternative to RSN that uses 1D projections for motion detection, image-based self-navigation offers similar efficiency and predictability while also enabling multi-dimensional motion correction.[14,49] That approach provided images of high diagnostic value in recent patient studies,[23,24] but validation in larger cohorts remains to be performed. Furthermore, approaches where both coronary anatomy and cardiac function can be captured in the same acquisition have been proposed,[50-52] which might facilitate the transition of CMRA into the clinics as conventional cine-imaging potentially could be replaced by such scans. However, further patient studies are needed with these recent techniques to identify CMRA protocols that handle the heterogeneity seen in patients and simultaneously come with tractable planning effort and practical acquisition and reconstruction times.

5 | CONCLUSIONS

Both the CNG and the RSN protocols proved adequate for identifying the position of all coronary ostia. However, the CNG protocol may be a better choice for examining vessel lumina because of its superior vessel conspicuity, given that the associated unpredictable and lengthy scan times can be accepted. RSN might be easier to include into comprehensive multi-sequence examinations because of its predictability and minimal planning effort. In addition, it may be considered more versatile given its isotropic resolution and more homogeneous blood signal. However, this direct comparison remains to be expanded to a real clinical setting.

CONFLICT OF INTEREST
The PhD studies of J.H. are supported financially by Siemens Healthcare (Erlangen, Germany). M.S. receives non-monetary research support from Siemens Healthcare (Erlangen, Germany). D.P. is an employee of Siemens Healthcare AG (Lausanne, Switzerland).

ORCID
John Heerfordt https://orcid.org/0000-0002-6837-4733
Matthias Stuber https://orcid.org/0000-0001-9843-2028
Davide Piccini https://orcid.org/0000-0003-4663-3244

REFERENCES

1. Kato S, Kitagawa K, Ishida N, et al. Assessment of coronary artery disease using magnetic resonance coronary angiography: a national multicenter trial. *J Am Coll Cardiol*. 2010;56:983–991.

2. Sakuma H, Ichikawa Y, Chino S, Hirano T, Makino K, Takeda K. Detection of coronary artery stenosis with whole-heart coronary magnetic resonance angiography. *J Am Coll Cardiol*. 2006;48:1946–1950.

3. Greenwood JP, Maredia N, Younger JF, et al. Cardiovascular magnetic resonance and single-photon emission computed tomography for diagnosis of coronary heart disease (CE-MARC): a prospective trial. *Lancet*. 2012;379:453–460.

4. Brittain JH, Hu BS, Wright GA, Meyer CH, Macovski A, Nishimura DG. Coronary angiography with magnetization-prepared T2 contrast. *Magn Reson Med*. 1995;33:689–696.

5. Rosen BR, Brady TJ. Selective saturation proton NMR imaging. *J Comput Assist Tomogr*. 1984;8:813–818.

6. Haase A, Frahm J, Hanicke W, Matthaei D. 1H NMR chemical shift selective (CHESS) imaging. *Phys Med Biol*. 1985;30:341–344.

7. Pruessmann KP, Weiger M, Scheidegger MB, Boesiger P. SENSE: sensitivity encoding for fast MRI. *Magn Reson Med*. 1999;42:952–962.

8. Griswold MA, Jakob PM, Heidemann RM, et al. Generalized autocalibrating partially parallel acquisitions (GRAPPA). *Magn Reson Med*. 2002;47:1202–1210.

9. Ehman RL, Felmlee JP. Adaptive technique for high-definition MR imaging of moving structures. *Radiology*. 1989;173:255–263.

10. McConnell MV, Khasgiwala VC, Savord BJ, et al. Prospective adaptive navigator correction for breath-hold MR coronary angiography. *Magn Reson Med*. 1997;37:148–152.

11. Ishida M, Schuster A, Takase S, et al. Impact of an abdominal belt on breathing patterns and scan efficiency in whole-heart coronary magnetic resonance angiography: comparison between the UK and Japan. *J Cardiovasc Magn Reson*. 2011;13:71.

12. Stehning C, Börnert P, Nehrke K, Eggers H, Stuber M. Free-breathing whole-heart coronary MRA with 3D radial SSFP and self-navigated image reconstruction. *Magn Reson Med*. 2005;54:476–480.

13. Deshpande VS, Chung YC, Zhang Q, Shea SM, Li D. Reduction of transient signal oscillations in true-FISP using a linear flip angle series magnetization preparation. *Magn Reson Med*. 2003;49:151–157.

14. Henningsson M, Koken P, Stehning C, Razavi R, Prieto C, Botnar RM. Whole-heart coronary MR angiography with 2D self-navigated image reconstruction. *Magn Reson Med*. 2012;67:437–445.

15. Pang J, Bhat H, Sharif B, et al. Whole-heart coronary MRA with 100% respiratory gating efficiency: self-navigated three-dimensional retrospective image-based motion correction (TRIM). *Magn Reson Med*. 2014;71:67–74.

16. Lustig M, Donoho D, Pauly JM. Sparse MRI: the application of compressed sensing for rapid MR imaging. *Magn Reson Med*. 2007;58:1182–1195.

17. Piccini D, Feng LI, Bonanno G, et al. Four-dimensional respiratory motion-resolved whole heart coronary MR angiography. *Magn Reson Med*. 2017;77:1473–1484.

18. Piccini D, Littmann A, Nielles-Vallespin S, Zenge MO. Respiratory self-navigation for whole-heart bright-blood coronary MRI: methods for robust isolation and automatic segmentation of the blood pool. *Magn Reson Med*. 2012;68:571–579.

19. Piccini D, Littmann A, Nielles-Vallespin S, Zenge MO. Spiral phyllotaxis: the natural way to construct a 3D radial trajectory in MRI. *Magn Reson Med*. 2011;66:1049–1056.

20. Piccini D, Monney P, Sierro C, et al. Respiratory self-navigated postcontrast whole-heart coronary MR angiography: initial experience in patients. *Radiology*. 2014;270:378–386.

21. Monney P, Piccini D, Rutz T, et al. Single centre experience of the application of self navigated 3D whole heart cardiovascular magnetic resonance for the assessment of cardiac anatomy in congenital heart disease. *J Cardiovasc Magn Reson*. 2015;17:55.

22. Albrecht MH, Varga-Szemes A, Schoepf UJ, et al. Coronary artery assessment using self-navigated free-breathing radial whole-heart magnetic resonance angiography in patients with congenital heart disease. *Eur Radiol*. 2018;28:1267–1275.

23. Henningsson M, Hussain T, Vieira MS, et al. Whole-heart coronary MR angiography using image-based navigation for the detection of coronary anomalies in adult patients with congenital heart disease. *J Magn Reson Imaging*. 2016;43:947–955.

24. Henningsson M, Shome J, Bratis K, Vieira MS, Nagel E, Botnar RM. Diagnostic performance of image navigated coronary CMR angiography in patients with coronary artery disease. *J Cardiovasc Magn Reson*. 2017;19:68.

25. Sakuma H, Ichikawa Y, Suzawa N, et al. Assessment of coronary arteries with total study time of less than 30 minutes by using whole-heart coronary MR angiography. *Radiology*. 2005;237:316–321.

26. Heerfordt J, Piccini D, Stuber M. A quantitative comparison of navigator-gated Cartesian and self-navigated radial free-breathing 3D bSSFP whole-heart coronary MRA. In Proceedings of a Joint EuroCMR/SCMR Meeting, Barcelona, Spain, 2018. Abstract #372044.

27. Wang Y, Riederer SJ, Ehman RL. Respiratory motion of the heart: kinematics and the implications for the spatial resolution in coronary imaging. *Magn Reson Med*. 1995;33:713–719.

28. Felmlee JP, Ehman RL. Spatial presaturation: a method for suppressing flow artifacts and improving depiction of vascular anatomy in MR imaging. *Radiology*. 1987;164:559–564.

29. Boada FE, Christensen JD, Gillen JS, Thulborn KR. Three-dimensional projection imaging with half the number of projections. *Magn Reson Med*. 1997;37:470–477.

30. Nielles-Vallespin S, Weber M-A, Bock M, et al. 3D radial projection technique with ultrashort echo times for sodium MRI: clinical applications in human brain and skeletal muscle. *Magn Reson Med*. 2007;57:74–81.

31. McConnell MV, Khasgiwala VC, Savord BJ, et al. Comparison of respiratory suppression methods and navigator locations for MR coronary angiography. *AJR Am J Roentgenol*. 1997;168:1369–1375.

32. Etienne A, Botnar RM, Van Muiswinkel AMC, Boesiger P, Manning WJ, Stuber M. "Soap-Bubble" visualization and quantitative analysis of 3D coronary magnetic resonance angiograms. *Magn Reson Med*. 2002;48:658–666.

33. Taylor AM, Jhooti P, Wiesmann F, Keegan J, Firmin DN, Pennell DJ. MR navigator-echo monitoring of temporal changes in diaphragm position: implications for MR coronary angiography. *J Magn Reson Imaging*. 1997;7:629–636.

34. Chaptinel J, Piccini D, Bonanno G, et al. Respiratory optimized data selection for more resilient self-navigated whole-heart coronary MR angiography. *MAGMA*. 2016;30:215–225.

35. Nehrke K, Börnert P, Manke D, Böck JC. Free-breathing cardiac MR imaging: study of implications of respiratory motion—initial results. *Radiology*. 2001;220:810–815.

36. Schmidt JFM, Buehrer M, Boesiger P, Kozerke S. Nonrigid retrospective respiratory motion correction in whole-heart coronary MRA. *Magn Reson Med*. 2011;66:1541–1549.

37. Ingle RR, Wu HH, Addy NO, et al. Nonrigid autofocus motion correction for coronary MR angiography with a 3D cones trajectory. *Magn Reson Med*. 2014;72:347–361.

38. Cruz G, Atkinson D, Henningsson M, Botnar RM, Prieto C. Highly efficient nonrigid motion-corrected 3D whole-heart coronary vessel wall imaging. *Magn Reson Med*. 2017;77:1894–1908.

39. McConnell MV, Ganz P, Selwyn AP, Li W, Edelman RR, Manning WJ. Identification of anomalous coronary arteries and their anatomic course by magnetic resonance coronary angiography. *Circulation*. 1995;92:3158–3162.

40. Albrecht MH, Varga-Szemes A, Schoepf UJ, et al. Diagnostic accuracy of non-contrast self-navigated free-breathing MR angiography versus CT angiography: a prospective study in pediatric patients with suspected anomalous coronary arteries. *Acad Radiol*. 2019;26:1309–1317.

41. Botnar RM, Stuber M, Kissinger KV, Manning WJ. Free-breathing 3D coronary MRA: the impact of "isotropic" image resolution. *J Magn Reson Imaging*. 2000;11:389–393.

42. Tandon A, Hashemi S, Parks WJ, Kelleman MS, Sallee D, Slesnick TC. Improved high-resolution pediatric vascular cardiovascular magnetic resonance with gadofosveset-enhanced 3D respiratory navigated, inversion recovery prepared gradient echo readout imaging compared to 3D balanced steady-state free precession readout imaging. *J Cardiovasc Magn Reson*. 2017;18:74.

43. Yang QI, Li K, Liu X, et al. Contrast-enhanced whole-heart coronary magnetic resonance angiography at 3.0-T. A comparative study with x-ray angiography in a single center. *J Am Coll Cardiol*. 2009;54:69–76.

44. Hu P, Chuang ML, Ngo LH, et al. Coronary MR imaging: effect of timing and dose of isosorbide dinitrate administration. *Radiology*. 2010;254:401–409.

45. Liu X, Bi X, Huang J, Jerecic R, Carr J, Li D. Contrast-enhanced whole-heart coronary magnetic resonance angiography at 3.0 T: comparison with steady-state free precession technique at 1.5 T. *Invest Radiol*. 2008;43:663–668.

46. Pang J, Sharif B, Arsanjani R, et al. Accelerated whole-heart coronary MRA using motion-corrected sensitivity encoding with three-dimensional projection reconstruction. *Magn Reson Med*. 2015;73:284–291.

47. Pruessmann KP, Weiger M, Börnert P, Boesiger P. Advances in sensitivity encoding with arbitrary k-space trajectories. *Magn Reson Med*. 2001;46:638–651.

48. Lustig M, Pauly JM. SPIRiT: iterative self-consistent parallel imaging reconstruction from arbitrary k-space. *Magn Reson Med*. 2010;64:457–471.

49. Luo J, Addy NO, Ingle RR, et al. Nonrigid motion correction with 3D image-based navigators for coronary MR angiography. *Magn Reson Med*. 2017;77:1884–1893.

50. Pang J, Sharif B, Fan Z, et al. ECG and navigator-free four-dimensional whole-heart coronary MRA for simultaneous visualization of cardiac anatomy and function. *Magn Reson Med*. 2014;72:1208–1217.

51. Coppo S, Piccini D, Bonanno G, et al. Free-running 4D whole-heart self-navigated golden angle MRI: initial results. *Magn Reson Med*. 2015;74:1306–1316.

52. Feng LI, Coppo S, Piccini D, et al. 5D whole-heart sparse MRI. *Magn Reson Med*. 2018;79:826–838.